MIT Libraries | DSpace@MIT

MIT Open Access Articles

A variable stiffness PZT cellular actuator with tunable resonance for cyclic motion tasks

The MIT Faculty has made this article openly available. ***Please share*** how this access benefits you. Your story matters.

Citation: Secord, T.W., and H.H. Asada. "A variable stiffness PZT cellular actuator with tunable resonance for cyclic motion tasks." Robotics and Automation, 2009. ICRA '09. IEEE International Conference on. 2009. 176-181. ©2009 IEEE.

As Published: http://dx.doi.org/10.1109/ROBOT.2009.5152288

Publisher: Institute of Electrical and Electronics Engineers

Persistent URL: http://hdl.handle.net/1721.1/60310

Version: Final published version: final published article, as it appeared in a journal, conference proceedings, or other formally published context

Terms of Use: Article is made available in accordance with the publisher's policy and may be subject to US copyright law. Please refer to the publisher's site for terms of use.

Massachusetts Institute of Technology

2009 IEEE International Conference on Robotics and Automation
Kobe International Conference Center
Kobe, Japan, May 12-17, 2009

A Variable Stiffness PZT Cellular Actuator with Tunable Resonance for Cyclic Motion Tasks

Thomas W. Secord *Student Member, IEEE* and H. Harry Asada, *Member, IEEE*

Abstract— **A simple and efficient approach for varying the inherent stiffness and impedance of a muscle-like actuator is presented. The basic architecture of PZT cellular actuators has already achieved a large effective strain (10-20%). This architecture is modified and extended so that each cellular unit can be switched between a zero compliance state and constant compliance state. The effective stiffness of the cellular actuator is varied by changing the distribution of cellular units in the rigid versus compliant state. Furthermore, by placing a multitude of these cellular units in series or parallel, the stiffness can vary within a large set of discrete values. This paper also demonstrates the viability of the variable stiffness cellular actuator for cyclic tasks such as running and flapping. The basic principle and design concept for the actuator is described, followed by force-displacement analysis. A dynamic model is then constructed to demonstrate the variable resonance properties of the actuator under load.**

I. Introduction

For the last three decades, a challenge within the robotics community has been to develop an actuator technology that can vary its inherent stiffness over a wide range and generate "natural" motions such as running, flapping, and jumping. Standard DC/AC motors with gearing cannot easily provide natural motions. Thus, there are two main challenges in actuator design for robotics: achieving variable stiffness and creating natural periodic motions.

The challenge of achieving variable stiffness has been studied by several groups. An explicit treatment of variable stiffness robotic finger joints began in the late 1980's and early 1990's (e.g. [1]). More recently, Hurst and Chestnutt [2] use inspiration from the spring-loaded inverted pendulum (SLIP) model [3] to propose a variable stiffness leg system. Variable stiffness joints are also important for safe human-robot interactions [4], [5]. One unifying theme in the literature is the use of traditional electromechanical actuators.

In the case of natural periodic motions such as running or flapping, it may be beneficial to operate the system at a resonant frequency. More specifically, resonance offers many important advantages for robotics applications:

- By definition, the resonant displacement amplitude of an actuator is larger than its static stroke, which is valuable for actuators having limited strain, such as PZT.
- When operating at resonance, the actuator's power efficiency and force transmissibility are excellent. This is an important property for mobile robots and other applications with limited energy sources.
- Control of the system is simplified in that the system is not required to be stable. More specifically, an ideal resonant system is unstable in a BIBO sense.

The idea of utilizing natural frequencies in robotic systems has its roots in the hopping robots of Raibert [6]. It has also been demonstrated that traditionally stiff actuators can resonate with the load by introducing a series elastic stiffness in the drive train [7]. More recently, flapping-flight robots have incorporated compliant elements to efficiently achieve desired wing rotation and flapping frequencies [8], [9]. The work in [10] and [11] explicitly maximizes resonance amplitude for piezoelectric materials and electrostrictive materials, respectively. Furthermore, animals, especially humans, prefer gait frequencies that closely correspond to the pendular resonant frequency of their limbs because it is energetically favorable and it appears to simplify the neural control of movement [12].

This paper presents a new design methodology for both variable stiffness and resonance by using actuators based on a cellular architecture. The cellular architecture is largely inspired by skeletal muscles, which consist of myriad small functional units. The philosophy of cellular architecture, as applied to robotic actuators, is to mass produce simple actuator units called cells and build an actuator using a collection of these cells [13], [14]. The collective properties and outputs of the actuator may then be varied by recruiting the necessary number of cells.

Presently, cellular architecture is applied directly to piezoelectric actuators. Piezoelectric materials, specifically PZT, exhibit high bandwidth, large stress capacity, and high efficiency. The major drawback of these materials is their small strain on the order of 0.1%. Recently, however, a technique has been developed to amplify the strain of PZT using a multiplicative effect based on nested flexure design [15]. The operating principle of the individual flexures is similar to the design in [16]. The resulting strains of prototype systems are over 20% and the bandwidth of a

T. W. Secord is a research assistant in the d'Arbeloff Laboratory for Information Systems and Technology. MIT Cambridge, MA 02139, USA. (phone: 617-253-3772; fax: 617-258-6575; e-mail: secord@mit.edu).

H Harry Asada is a Ford Professor of Mechanical Engineering at MIT Cambridge, MA 02139, USA.

single actuator unit is over 60 Hz [17]. This paper greatly extends the authors' previous work in cellular architecture and shows, for the first time, its usefulness in variable stiffness and variable resonance systems.

Section II of this paper presents the concept for PZT variable stiffness cellular actuators (PZT-VSCA) and Section III will address the dynamics of variable stiffness cellular actuators with an emphasis on resonance. The analysis will show that switching between numerous combinations of individual cell states can generate diverse stiffness levels and resonant frequencies that meet task specifications.

II. Principles of Variable Stiffness PZT-CA

A. Design Concept

Fig. 1 shows the concept of nested-flexure PZT cellular actuation. Fig. 1-(a) shows a prototype of serially connected PZT cellular actuators. The six cellular units connected in series yield a 65 mm net body length that can produce 7 mm total free displacement and a 5 N blocking force. Each cellular unit (shown in Fig. 1-(b)) consists of a pair of PZT stacks and double-layer nested flexures that amplify the PZT displacement by a combined factor of 20.

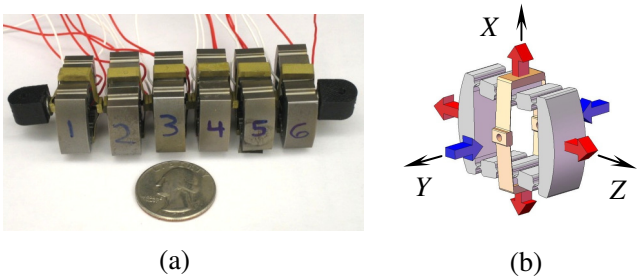

Fig. 1. (a) Nested PZT cellular actuator having 6 serially connected cells. (b) Motion of nested amplification flexures. PZT stacks removed for clarity.

As a voltage is applied to the PZT stacks, the first layer flexure is pushed outward along the Z direction, which results in an outward amplified displacement in the X direction. The second layer flexure is also pushed outward in the X direction, which results in a further amplified displacement in the inward Y direction. Therefore, a contraction force is generated along the Y-axis output as the PZT stacks are activated. This contractile double-layer flexure design allows the connection of multiple units in series without buckling.

Fig. 2 shows a modification to the above design. Outside the second layer flexure is a rigid structure that limits the stroke of the output displacement in the Y direction. When the PZT is not activated, the output node of the second layer flexure rests on the stroke limiting beam. The output node movement is also limited when an excessive tensile force acts on the output node. As the applied PZT voltage increases, the output node is pulled inward and is detached from the stroke limiting beam.

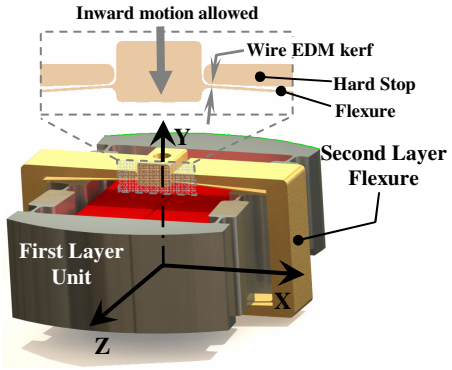

Fig. 2. Design of a variable stiffness PZT-based cell. The system consists of two strain amplified layers. The second layer flexure incorporates flexure hard stops.

Fig. 3 is a schematic diagram depicting the mechanism of the cellular unit with a stroke limiter. The thick black lines indicate the stroke limiter, while the vertical grey lines show the output nodes of the flexure that rest on the stroke limiter when the PZT is inactive. Each side of the flexure shown in Fig. 2 is modeled with a lumped stiffness k in Fig. 3. As the PZT induced force f_p increases, the vertical grey lines are detached from the limiter.

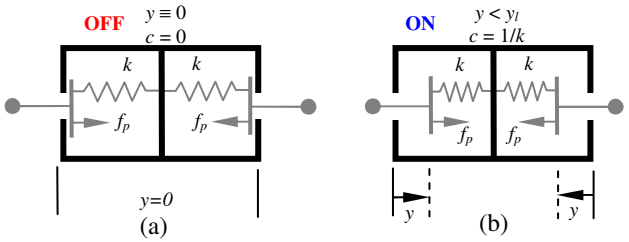

Fig. 3. Schematic model of a variable stiffness, PZT-actuated cell. (a) OFF–strain limited rigid state. (b) ON – compliant state.

The compliance characteristics associated with the cellular unit are shown in Fig. 4. The compliance is variable in the sense that it can be either zero or some finite value $c = 2/k$. For simplicity of analysis, it is assumed that the compliance follows the ideal solid line curve. In reality, the hard stop imposed by the flexure still affords some finite compliance c_f. Furthermore, the compliance will actually increase as the cell becomes contracted due to the geometric nonlinearity of the flexure. The nonlinearity is assumed to be negligible within the operation range $0 < y < y_l$.

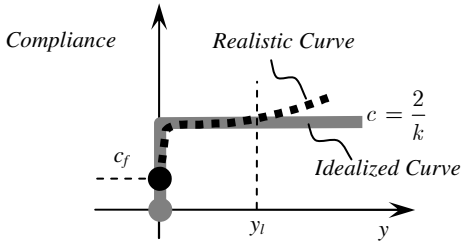

Fig. 4. Compliance characteristics of a variable stiffness PZT-actuated cell.

B. Stiffness Variation for an Array of Cells

Fig. 5 shows an array of the cells considered in Fig. 3. The array of cells is described with a serial index i and a parallel

index *j*. The equivalent stiffness of the parallel assembly is given by

$$k_{eq} = \sum_{j=1}^{N_p} \frac{k}{2(N_s - N_{OFF,j})}, \quad (1)$$

where $N_{OFF,j}$ is the number of units in the *j*th branch which are OFF.

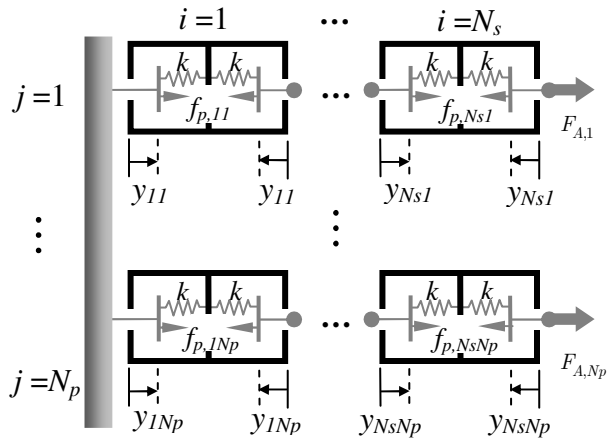

Fig. 5. Serial and parallel connection of variable stiffness cells. The total tensile force is F_A is split between the N_p branches in the assembly.

Eq. (1) shows that the equivalent stiffness of the entire assembly can be tuned to various values by recruiting the appropriate numbers of cells for each serial connection. Notice that the equivalent stiffness of a branch is uniquely determined by the number of OFF units in that branch. For a given array of ON-OFF units, the distribution of recruited cells (ON state cells) must satisfy certain conditions to meet the total force and displacement requirements. These requirements will be analyzed in the following section.

C. Static Force-Displacement Analysis

For a general parallel connection, let $f_{p,ij}$ be the internally generated piezo force and V_{ij} the voltage applied to the piezo stacks of the *ij*th unit. The piezo force is modeled with the linear relationship

$$f_{p,ij} = \beta_1 V_{ij} - \beta_2 y_{ij}, \quad (2)$$

where β_1 is the voltage to force transduction constant for each cell, which depends upon the amplification flexure design and the material. β_2 is an equivalent parallel stiffness that determines the maximum allowable inward displacement of the force generator in each cell.

The force $F_{A,j}$ in each branch consists of a strictly tensile preload force $F_{PL,j}$ and an allowable bipolar deviation from the preload $\tilde{F}_j$. That is, $F_{A,j} = F_{PL,j} + \tilde{F}_j$, where $|\tilde{F}_j| < F_{PL,j}$ is needed to avoid losing the preload and allowing the OFF cells to become slack. Furthermore, $\sum_j \tilde{F}_j = \tilde{F}$, $\sum_j F_{PL,j} = F_{PL}$, and $F_A = F_{PL} + \tilde{F}$.

In order for an individual cell to be ON, the applied voltage must satisfy the inequality

$$V_{\min,j} = \frac{\tilde{F}_j + F_{PL,j}}{\beta_1} < V_{ij} < V_{\max}^{PZT}. \quad (3)$$

Eq. (3) shows that for a cell to be ON it must have a minimum voltage applied dependent upon the branch force and this voltage must be less than the maximum allowable voltage $V_{\max}^{PZT}$ where depolarization of the PZT material occurs. If (3) is satisfied for the ON cells and the total contractile displacement Y_T is taken as the same for each branch, then

$$Y_T = \sum_{i=1}^{N_s} 2\alpha_{ij} \frac{\beta_1 V_{ij} - (\tilde{F}_j + F_{PL,j})}{k + \beta_2}, \quad (4)$$

where α_{ij} is the activation Boolean defined by

$$\alpha_{ij} = \begin{cases} 0 & V_{ij} < V_{min,j} \\ 1 & V_{ij} \geq V_{min,j} \end{cases}. \quad (5)$$

The maximum total displacement ($\alpha_{ij} = 1$ for all *i*, *j*) is given by

$$Y_{T,\max} = \frac{2N_s}{k + \beta_2}\left(\beta_1 V_{max}^{PZT} - \frac{\tilde{F} + F_{PL}}{N_p}\right). \quad (6)$$

Observe that the maximum total displacement is proportional to N_s, β_1, and $V_{\max}^{PZT}$, but it is inversely proportional to β_2 and *k*. Furthermore, if the total actuator load F_A is borne by several units in parallel, then $Y_{T,\max}$ will also increase.

One may envision a host of other connection topologies for the PZT-VSCA. Each connection topology must satisfy a set of excitation and kinematic constraints (i.e. capability to turn ON and avoiding hitting the hard stops). The constraint equations previously formulated for parallel arrangements may be readily extended to include other connections.

III. Application of PZT-CA to Resonant Systems

In the previous section, the actuator relationships were developed for static equilibrium and low frequency motion (e.g. a decade below the first resonance of the assembled system). In this section, the variable stiffness actuator is described in terms of its dynamic, rather than static, properties.

One unifying trait among robotic systems is that task space motions are often periodic. The requirement for repetitive motion is especially apparent in the field of mobile robots, where energy efficiency is paramount in the design. When the frequency content of a robot's motion lies within a narrow band, then it may be beneficial to utilize mechanical resonance to dynamically amplify displacements and improve efficiency. To elucidate the key design parameters, a single cell dynamic model is formulated and then extended to include serial connection dynamics.

A. *Single Cell Dynamic Model*

The general model shown in Fig. 3 for an individual cell must be modified to account for the differential displacement and mass m that become prominent model parameters near resonance. The augmented schematic model of the cell is shown in Fig. 6. The mass m in the figure is rigidly situated inside the stroke limiting mechanism and the displacements are given subscripts p and d to indicate proximal and distal, respectively. The proximal displacement is the displacement closer to the ground connection point, while the distal displacement is closer to the load connection point.

The same conditions in (3) must still be satisfied by each ON cell, but the required caveat is that $\tilde{F}$ now arises from time varying d'Alembert forces. Hence, a larger preload may be required to avoid OFF cells experiencing zero net tension. For simplicity of analysis, it is assumed that all cells encounter only net tensile forces and that the minimum voltage requirement is met for ON cells.

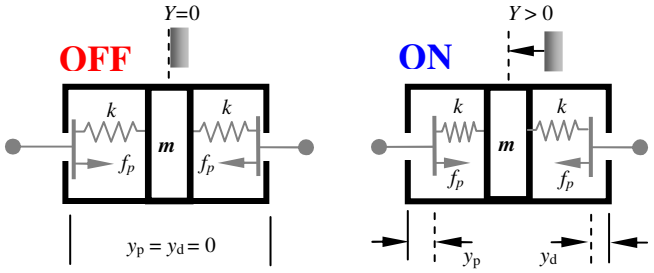

Fig. 6. Dynamic model of a VSCA-PZT that includes mass and differential displacement.

B. *Serial Connection Clustering and Dynamics*

The model in the previous subsection is now analyzed within a cellular assembly. For any VSCA arrangement, the dynamic behavior of the actuator and load can vary significantly depending upon the distribution of ON-OFF states. This trait is central to the VSCA approach. For clarity, the discussion of resonance tuning is restricted to serial connections. However, the following analysis may be readily extended to include parallel and antagonistic connections. In order to correctly establish the generalized coordinates for a serial connection of cells, the cells must first be grouped or clustered according to the activation states α_i.

As an example of the clustering scheme, consider the serial connection in Fig. 7. The cluster index is denoted by q with the total number of clusters denoted by N_c. The cluster set is defined as the ordered indices of the cells in the cluster. Each cluster receives a generalized coordinate Y_q. Fig. 7 shows that the first cell in the chain (i = 1) is OFF (α_1= 0) and it is connected directly to ground. Therefore, this cell does not participate dynamically but instead moves the ground to the point between cells 1 and 2. Thus, cell 1 is not counted as a cluster. Cell 2 is ON and therefore cell 2 participates as both a mass and stiffness as shown in the right hand portion of Fig. 6. Cells 3 and 4 are both OFF, which implies that they translate together as a mass $2m$.

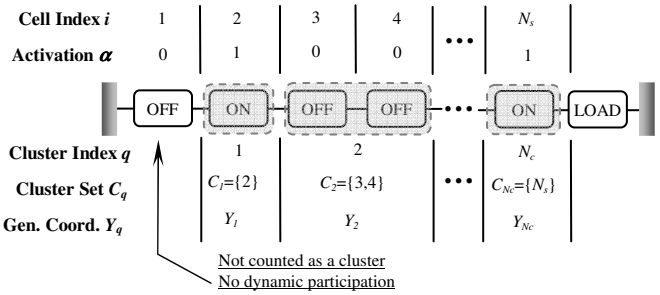

Fig. 7. Example of clustering scheme used to quantify the system mass and stiffness properties.

Finally, the last unit in the chain, cell N_s, is ON and this cell behaves as both a mass and stiffness. It is interesting to note that this system will have the same static behavior as any other system having the same number of OFF units. However, the appropriate clustering of cells must be performed because both the dynamics and system order are highly dependent upon this grouping.

Once the clustering is complete, the system will be represented as shown in Fig. 8. To facilitate the discussion, the load on the actuator will be a mass m_L connected to the ground through a linear spring k_L. Also in Fig. 8, the coordinate Y_L has been introduced to characterize the load position for the case when α_{Ns} = 1. The notation $n(C_q)$ denotes the cardinality of the qth cluster set, which determines the equivalent mass that the cluster contributes to the kinetic energy. The interconnection stiffness k_q may be established from the following logic expression:

$$k_q = \begin{cases} k & q = 1 \\ \frac{k}{2} & q > 1 \wedge (\alpha_i \in C_{q-1}) = 1 \wedge (\alpha_i \in C_q) = 1 \\ k & q > 1 \wedge (\alpha_i \in C_{q-1}) = 0 \wedge (\alpha_i \in C_q) = 1 \end{cases}. \tag{7}$$

The elastic potential energy V in the system is the sum of an internal energy term V_I and an energy term V_B that depends upon the state of the last cell in the serial chain. The internal energy is

$$V_I = \frac{1}{2}k_1 Y_1^2 + \frac{1}{2}\sum_{q=2}^{N_c} k_q (Y_q - Y_{q-1})^2 \tag{8}$$

and the boundary energy is

$$V_B = \begin{cases} \frac{1}{2}k(Y_L - Y_{Nc})^2 + \frac{1}{2}k_L Y_L^2 & \text{if } \alpha_{Ns} = 1 \\ \frac{1}{2}k_L Y_{Nc}^2 & \text{if } \alpha_{Ns} = 0 \end{cases}. \tag{9}$$

Similarly, the kinetic energy T is the sum of an internal energy term T_I and a boundary term T_B, where

$$T_I = \frac{1}{2}\sum_{q=1}^{N_c - 1} n(C_q) m \dot{Y}_q^2 \tag{10}$$

and

$$T_B = \begin{cases} \frac{1}{2}m\dot{Y}_{Nc}^2 + \frac{1}{2}m_L\dot{Y}_L^2 & \text{if } \alpha_{Ns} = 1 \\ \frac{1}{2}\left(n(C_{Nc})m + m_L\right)\dot{Y}_{Nc}^2 & \text{if } \alpha_{Ns} = 0 \end{cases}. \tag{11}$$

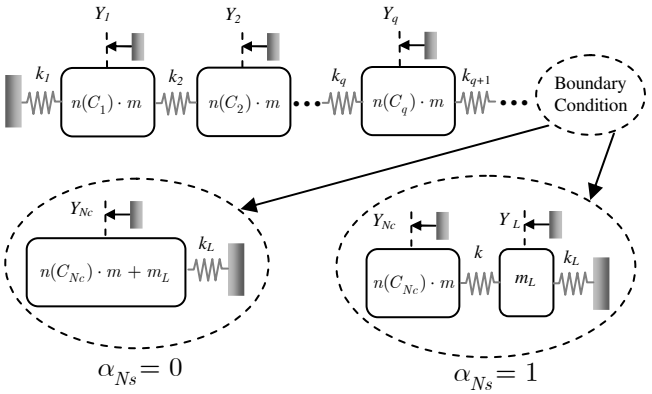

Fig. 8. System description after clustering has been performed. $n(Cq)$ denotes the cardinality or size of the qth cluster set.

The total mechanical energy, given by the sum of (8) to (11), is sufficient to obtain all of the system natural modes. Denoting the generalized coordinate vector by $\{\mathbf{Y}\}$, the system stiffness and mass matrices are the Hessians

$$[\mathbf{M}] = \frac{\partial^2 T}{\partial \{\mathbf{Y}\}^2} \quad \text{and} \quad [\mathbf{K}] = \frac{\partial^2 V}{\partial \{\mathbf{Y}\}^2}. \tag{12}$$

In general, the serially connected system may exhibit N_c natural modes when $\alpha_{Ns} = 0$ and $N_c + 1$ natural modes when $\alpha_{Ns} = 1$. Although a large number of modes may exist, the fundamental frequency ω_{n1} and fundamental mode shape are of the most design relevance. Therefore, after obtaining the matrices in (12), the first eigenvalue and first right eigenvector of the dynamic matrix $[\mathbf{M}]^{-1}[\mathbf{K}]$ are readily obtained for use in design.

C. Design Example

As an example of serial connection dynamic behavior, consider Fig. 9, which shows all possible combinations of ON-OFF states for three cells connected to a spring-mass load.

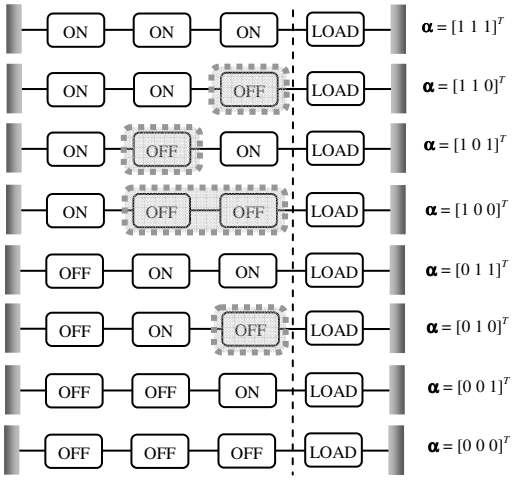

Fig. 9. Example where $N_s = 3$ and the units are connected to a spring-mass load. The clusters of OFF units are marked with dashed line boxes.

Within Fig. 9, consider the case where $\alpha = [1\ 0\ 0]^T$. The two cells closest to the load are connected rigidly when they are in the OFF state and therefore they participate in the dynamic motion only as mass $2m$. Moreover, the dynamics for $\alpha = [1\ 0\ 0]^T$ is third order while the base case $\alpha = [1\ 1\ 1]^T$ is fourth order because all mass and stiffness elements are active in the system.

A dimensionless stiffness $\bar{k}$ is defined as the individual flexure stiffness normalized by the load stiffness: $\bar{k} \triangleq k / k_L$. Likewise, the dimensionless mass is the mass of a cell normalized by the load mass: $\bar{m} \triangleq m / m_L$. Note that $\bar{k}$ and $\bar{m}$ are parameters determined by the flexure design and the properties of the driven load.

Table 1 shows the first natural frequency of the systems in Fig. 9 relative to the original system fundamental frequency $\omega_{n1}/\omega_{n,L}$ where $\omega_{n,L}^2 = k_L / m_L$. Three different cases for $\bar{k}$ and $\bar{m}$ are shown in the table.

TABLE I
VARIATIONS IN THE FUNDAMENTAL FREQUENCY OF A THREE CELL SYSTEM

Case, α	$\bar{k} = 0.1$ $\bar{m} = 0.5$	$\bar{k} = 0.1$ $\bar{m} = 0.1$	$\bar{k} = 0.5$ $\bar{m} = 0.1$
	$\omega_{n1}/\omega_{n,L}$	$\omega_{n1}/\omega_{n,L}$	$\omega_{n1}/\omega_{n,L}$
[1 1 1]	0.31	0.69	1.44
[1 1 0]	0.44	0.97	1.91
[1 0 1]	0.33	0.75	1.53
[1 0 0]	0.31	0.67	0.96
[0 1 1]	0.35	0.74	0.87
[0 1 0]	0.60	0.96	1.05
[0 0 1]	0.61	1.00	1.10
[0 0 0]	NA	NA	NA

Assume that the original load and actuator combination has $\bar{k} = 0.5$ and $\bar{m} = 0.1$. Also, suppose that the inherent resonant frequency of the load must be increased by 91% to achieve the desired output periodic motion. From Table I, with $\alpha = [1\ 1\ 0]^T$, the first natural frequency of the system does indeed increase by 91% over the load's inherent natural frequency. Taking m_L as 300 g and k_L as 0.8 N/mm, the flexure system must be designed so that each unit has m = 30 g and k = 0.4 N/mm. These values are representative of the current cellular actuator prototype. The inherent natural frequency of the load is 51.6 rad/s while the desired resonant frequency is 91% higher at 98.9 rad/s. A centralized controller then imposes the state $\alpha = [1\ 1\ 0]^T$ and excites the system at the new resonant frequency using $V_{pzt}(t) = V_o \sin(\omega_{n1} t)$, where V_o is selected to simultaneously achieve the desired output amplitude and satisfy the constraint in (3).

The theoretical results of the frequency response from input piezo force to output load displacement are shown in Fig. 10. Notice that the fully assembled system has three natural modes because there are three clusters and the unit adjacent to the load is OFF. This example has shown that the

resonant frequency of an actuated system may be widely tuned by simply changing the frequency of the driving input and the set of activation states. This variable resonance behavior allows the actuator to meet wide ranging design specifications for the motion output.

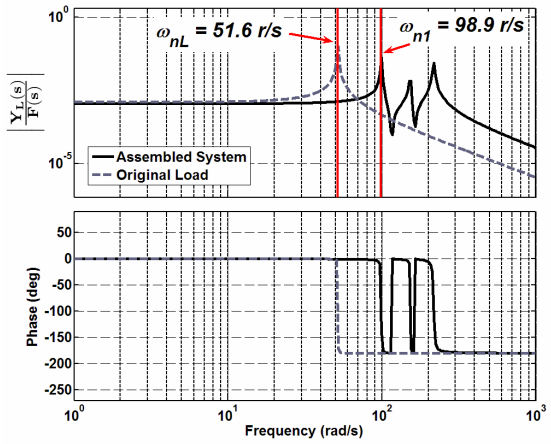

Fig. 10. Frequency response for the design having N_s = 3, m_L = 300 g, k_L = 0.8 N/mm, and a desired increase in load resonance of 91%.

IV. Conclusions

The design presented in this paper uses a novel concept of a PZT-VSCA. The procedures and relations presented are broadly applicable to variable stiffness static systems as well as resonant systems undergoing periodic motion. Models and design examples have been used to illustrate the approach and to motivate further study and experimentation.

In the first portion of the paper, the PZT-VSCA was shown to meet low frequency demands for variations in equivalent stiffness. The equivalent stiffness is determined by the number of OFF units in an actuator strand. In the second portion of the paper, the actuators were shown to meet high frequency demands for both variable stiffness and inertia. The proposed design uses the inherent compliance and mass properties of the actuator along with different cell recruitment patterns to vary the dynamic properties of the loaded system. The analysis demonstrated that a useful application of the actuators is to tune a resonant frequency to meet design specifications (e.g. a percentage increase or decrease in the inherent load natural frequency). Even under changes in load structure or properties, the output motion amplitude can be tuned to a resonance condition so that the dynamic load displacement greatly exceeds its static amplitude. This approach is especially appealing because power consumption and force transmissibility are excellent when operated under the resonance condition. A forthcoming publication will include the experimental results augmenting the theory presented in this paper.

References

[1] S. Sugano, S. Tsuto, and I. Kato, "Force Control of the Robot Finger Joint Equipped with Mechanical Compliance Adjuster", *Proc. of the 1992 IEEE/RSJ Int. Conf. on Intelligent Robots and Systems*, pp. 2005-2013, 1992.

[2] J. Hurst, J. Chestnutt, and A. Rizzi, "An Actuator with Physically Variable Stiffness for Highly Dynamic Legged Locomotion", *Proc. of IEEE Int. Conf. on Robotics and Automation*, pp. 4662-4667, 2004.

[3] R. Blickhan, "The Spring-Mass Model for Running and Hopping", *Journal of Biomechanics*, Vol. 22, No. 11/12., pp. 1217-1227, 1989.

[4] J. Choi, S. Park, W. Lee, and S. Kang, "Design of a Robot Joint with Variable Stiffness", *Proc. of IEEE Int. Conf. on Robotics and Automation*, pp. 1760-1765, 2008.

[5] R. Schiavi, G. Grioli, S. Sen, and A. Bicchi, "VSA-II: A Novel Prototype of Variable Stiffness Actuator for Safe and Performing Robots Interacting with Humans", *Proc. of IEEE Int. Conf. on Robotics and Automation*, pp. 1760-1765, 2008.

[6] M. Raibert, "Legged Robots That Balance", Cambridge, MA: MIT Press, 1986.

[7] G. Pratt and M. Williamson, "Series Elastic Actuators", *Proc. of IEEE/RSJ Int. Conf. on Intelligent Robots and Systems*, Vol. 1, pp. 399-406, 1995.

[8] J. Yan, R. Wood, S. Avandhanula, M. Sitti, and R. Fearing, "Towards Flapping Wing Control for a Micromechanical Flying Insect", *Proc. of IEEE Int. Conf. on Robotics and Automation*, pp. 3901-3908, 2001.

[9] K. Issac and S. Agrawal, "An Investigation Into the Use of Springs and Wing Motions to Minimize the Power Expended by a Pigeon-Sized Mechanical Bird for Steady Flight", *J. Mech. Design*, Vol. 129, pp. 381-389, 2007.

[10] N. Lobontiu, M. Goldfarb, and E. Garcia, "Maximizing the Resonant Displacement of Piezoelectric Beams", *Proc. SPIE*, Vol. 3668, No. 154, 1999.

[11] R. Kornbluh, R. Pelrine, J. Eckerle, and J. Joseph, "Electrostrictive Polymer Artificial Muscle Actuators", *Proc. of IEEE Int. Conf. on Robotics and Automation,* Vol. 3, pp.2147-2154, 1998.

[12] L. Goodman, M. Riley, and S. Mitra, and M. Turvey, "Advantages of Rhythmic Movements at Resonance: Minimal Active Degrees of Freedom, Minimal Noise, and Maximal Predictability", *Journal of Motor Behavior*, Vol. 32, No. 1, pp 3-8, 2000.

[13] J. Ueda, L. Odhner, and H. Asada, "Broadcast Feedback of Stochastic Cellular Actuators Inspired by Biological Muscle Control", *The Int. Journal of Robotics Research,* Vol. 26, No. 11-12, pp. 1251-1265, 2007.

[14] K. Cho, J. Rosmarin, and H. Asada, "Design of Vast DOF Artificial Muscle Actuators with a Cellular Array Structure and its Application to a Five-fingered Robotic Hand", *IEEE Int. Conf. on Robotics and Automation*, pp. 2214-2219, 2006.

[15] J. Ueda, T. Secord, and H. Asada, "Design of PZT Cellular Actuators with Power-law Strain Amplification", *Proc. of IEEE/RSJ Int. Conf. on Robots and Systems*, pp. 1160-1165, 2007.

[16] A. Dogan, K. Unchino, and R.E. Newnham, "Composite Piezoelectric Transducer with Truncated Conical Endcaps, Cymbal", *IEEE Trans. on Ultrasonics, Ferroelectrics, and Frequency Control*, Vol. 44, pp. 597-605, 1997.

[17] T. Secord, J. Ueda, and H. Asada, "Dynamic Analysis of a High Bandwidth, Large-Strain, PZT Cellular Muscle Actuator with Layered Strain Amplification", *Proc. of IEEE Int. Conf. on Robotics and Automation*, pp. 761-766, 2008.